Decomposition and nanocrystallization in reactively sputtered amorphous Ta–Si–N thin films

C. U. Pinnow,[a] M. Bicker, U. Geyer, and S. Schneider
Universität Göttingen, I. Physikalisches Institut, Bunsenstrasse 9, Göttingen, Germany

G. Goerigk
Forschungszentrum Jülich GmbH, Institut für Festkörperforschung, Jülich, Germany

(Received 1 February 2001; accepted for publication 1 June 2001)

The nanocrystallization process of reactively sputtered thin amorphous Ta–Si–N films is investigated by anomalous small angle x-ray scattering (ASAXS) and x-ray diffraction (XRD). Changes in the microstructure in $Ta_{40}Si_{14}N_{46}$ films, density variations in the amorphous matrix, decomposition, formation, and growth of nanocrystals after vacuum anneals at different temperatures in the range between 800 and 1000 °C are observed and the results of the different techniques are compared. From a Fourier analysis of ASAXS intensities the nanostructure of the investigated ternary system is derived using a model of hard spheres according to Guinier and Fournet. ASAXS investigations indicate that the noncrystalline samples can be described by a monophase fit and the crystallized samples by a bimodal-phase fit, the latter results being consistent with XRD which identifies TaN and Ta_5Si_3 phases. Detailed analysis shows that TaN nanograins of approximately 2 nm size develop after a decomposition process. Larger grains of Ta_5Si_3 are observed in addition to the TaN grains if annealing is performed at temperatures higher than 950 °C. The aim of these investigations is to give a generally applicable explanation of the barrier failure mechanism for Ta–Si–N diffusion barriers, which is actually observed at temperatures below the crystallization temperature if the films are used in contact with Cu or Al. © *2001 American Institute of Physics.* [DOI: 10.1063/1.1388173]

I. INTRODUCTION

Though Cu shows superior electrical properties in comparison to Al in Si-based integrated circuits, such as lower resistivity and improved electromigration behavior, the integration of Cu is challenging because of the problem of its high diffusivity in Si. Therefore it is necessary to develop effective diffusion barriers for Cu metallizations. By diffusion along grain boundaries of polycrystalline TiN[1,2] and TaN[3,4] barrier films Al and Cu can penetrate these films, and the functionality of the devices is lost due to deep trap formation in the semiconductor material or even chemical reactions such as formation of metal silicides. These reactions can be delayed by barrier stuffing or texture control[5] of TiN films, but not effectively suppressed at temperatures higher than about 650 °C for longer annealing times. One of the most promising barrier film materials overcoming these problems is amorphous Ta–Si–N.[6–8] Besides the use of Ta–Si–N films as barrier layers for Cu metallizations, they have been investigated as a material against oxygen diffusion in volatile and nonvolatile memory (dynamic random access memory/Ferroelectric RAM)[9–12] and other applications such as transducer and primary masks for x rays.[13]

As Cu diffusion barriers these ternary amorphous films are more suitable than polycrystalline materials because of the absence of grain boundaries,[14] their high thermal stability against crystallization, and lower intrinsic compressive stress compared to TaN_x.[15] This indicates that the stability of the amorphous structure of these films determines their properties and feasibility of integration in semiconductor devices. Consequently, the microstructure of the films on a nanometer scale should be the subject of a more detailed investigation. For this purpose a combination of small angle scattering methods and conventional x-ray diffraction analysis are chosen to detect possible changes in the amorphous matrix. Due to the geometry and the possibility of energy variation in the small angle x-ray scattering analysis this method yields valuable data about the structural and chemical properties of the sample on a length scale ranging from one to several tens of nanometers. Moreover, small angle x-ray scattering (SAXS) and x-ray diffraction (XRD) are complementary methods, since SAXS data contains information about the lateral (in plane) size of the scatterers in the sample.

Recent stability studies of diodes containing amorphous Ta–Si–N diffusion barriers have shown that the failure temperatures, T_f, of Cu/Ta–Si–N/Si stacks are about 700–825 °C, depending on film composition.[16] The failure mechanism itself is still unknown, since some of the investigated barriers stay amorphous until failure temperature is reached. It is the aim of the present paper to illuminate the interrelation between barrier failure and the first stages of microstructural changes in the amorphous matrix of $Ta_{40}Si_{14}N_{46}$ samples.

II. EXPERIMENT

The Ta–Si–N films were reactively rf sputtered from a Ta_5Si_3 target in an Ar/N_2 gas mixture at a sputtering power

[a]Electronic mail: cpinnow@gwdg.de

TABLE I. Abbreviations used for the investigated $Ta_{40}Si_{14}N_{46}$ samples.

Sample name	$Ta_{40}Si_{14}N_{46}$ sample, annealing conditions
A	as-prepared
B	800 °C, 1 h
C	850 °C, 1 h
D	900 °C, 1 h
E	950 °C, 1 h
F	1000 °C, 1 h

of $P=300$ W. As substrates Si(100) wafers with a thickness of $d_{Si}=30$ μm with a native oxide were chosen. Film thickness was $d_f=750$ nm on each side of the substrate in order to improve scattering yield for SAXS studies. Six different samples were analyzed, the as-prepared and five furnace-annealed samples, the latter ones were annealed in steps of 50 °C in a temperature range from 800 to 1000 °C in Ar atmosphere for 1 h. The so-prepared samples are named with the letters A–F as shown in Table I. X-ray diffraction data was recorded with a PHILIPS PW 1050/25 diffractometer in Bragg–Brentano geometry.

Anomalous small angle x-ray scattering (ASAXS) measurements were performed at the JUSIFA beamline at HASYLAB/DESY in Hamburg.[17] The scattering intensities were measured between $q_{min}=0.006$ Å^{-1} and $q_{max}=0.6$ Å^{-1}, q being the modulus of the scattering vector $\mathbf{q}=\mathbf{k}-\mathbf{k}_0$, $\mathbf{k}$ and $\mathbf{k}_0$ are the wave vector of the scattered and the incident waves, respectively. The scattering angle 2θ is related to q by the equation $q=4\pi/\lambda \sin\theta$, where λ is the wavelength of the used radiation. The presented radial scattering data was calculated by azimuthally integrating the measured two-dimensional (2D) intensities in finite q slices.

The recorded scattering curves contain information about the inhomogeneities of the investigated samples, i.e., size, shape, size distribution, volume fraction, and chemical composition. The data was background-corrected and an absolute calibration to electron units (e.u./TaSiN) was done by comparing the scattering intensity to that of a glassy carbon (GC) reference sample.

Small angle scattering at a certain fixed energy cannot distinguish whether scattering contrast is produced by pores or by particles of a second phase which develops in the matrix. Multicomponent films with different particle sizes and/or shapes are even more difficult to analyze because scattering intensities of all phases add up and superimpose. To prove that scattering contrast arises from scattering due to a difference in Ta concentration, anomalous scattering experiments were done and incident photon energies were varied just below the Ta-L_{III} edge ($E_{Ta,L_{III}}=9881$ eV). Resonant scattering of L electrons changes $f'(E)$ in the atomic form factor given by $f(E,Z)=f_0+f'(E)+if''(E)$, where $f''(E)$ is directly proportional to the absorption coefficient $\mu(E)$ and $f_0\to Z$ if $q\to 0$. The separated scattering intensities were calculated by subtracting the scattering curve measured at $E=9876$ eV from that measured at $E=9682$ eV.

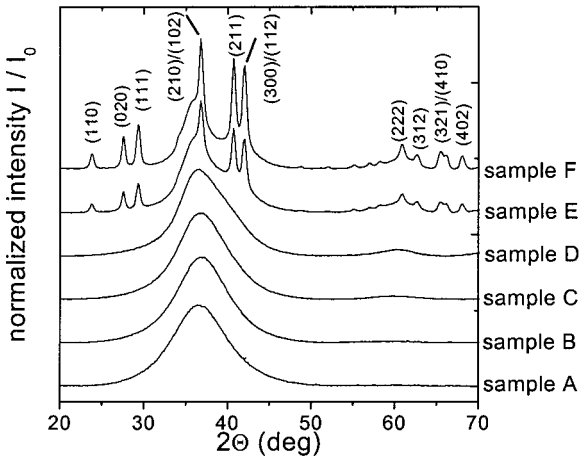

FIG. 1. Wide angle x-ray spectra of $Ta_{40}Si_{14}N_{46}$ samples annealed in Ar atmosphere for 1 h at different temperatures. The indexed reflexes occurring at 950 and 1000 °C are reflexes of the hexagonal Ta_5Si_3 phase.

III. RESULTS AND DISCUSSION

A. X-ray-diffraction analysis

Lorentzian curves were fitted to the peaks in the diffraction spectra presented in Fig. 1 and the observed full width at half maximum (FWHM) was used to determine the vertical coherence length, d_{coh}, which estimates the vertical grain size in (partly) crystalline samples. For this calculation the Scherrer formula was used

$$d_{coh}=0.9\lambda/(B\cos\theta), \tag{1}$$

where λ is the wavelength of the used Cu K_α radiation and B is the FWHM of the observed peak.[18] The data calculated from Eq. (1) for the coherence length is summarized in Table II as d_{coh}, however, the values should be regarded as estimations due to the size and shape distribution of the crystalline particles. The wide angle x-ray studies show that crystalline nanograins have developed in the samples E and F. The sharp peaks indexed in Fig. 1 all belong to the hexagonal Ta_5Si_3 phase with grain sizes for the x-ray-crystalline samples E and F of $d_{coh}=16-20$ nm. Additionally there are broad peaks visible in the spectra of these two crystalline samples, which can be identified to be caused by very small grains ($d=2.5-4$ nm) of a cubic TaN phase and a residual amorphous phase that should be present in these samples.

The spectrum of sample D shows a slight asymmetry of the broad maximum at $2\theta\approx 36°$, and in addition to that a

TABLE II. Particle sizes calculated from *C(r)*, by Guinier fits and XRD results.

$Ta_{40}Si_{14}N_{46}$ sample	D_{max} from $C(r)=$min. (nm)	$D_K=2R_K=2\sqrt{5/3}R_G$ (nm)	d_{coh} (TaN) (nm)	d_{coh} (Ta_5Si_3) (nm)
A	1.2		1.1	1.1
B	1.6		1.5	1.5
C	1.8		1.7	1.7
D	1.9		2.1	
E	2.5	16.3±0.6	2–3	16–20
F		17.1±0.6	2.5–4	16–20

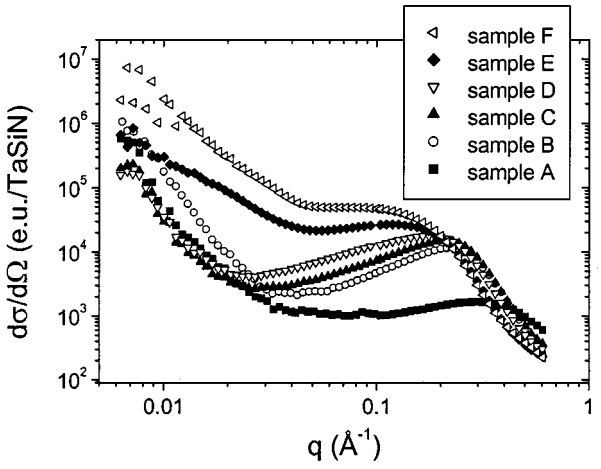

FIG. 2. Radial scattering intensities from six different $Ta_{40}Si_{14}N_{46}$ samples (A–F). Scattering curves were background corrected, normalized, and combined at $q=0.1$ Å^{-1}, $E=9682$ eV.

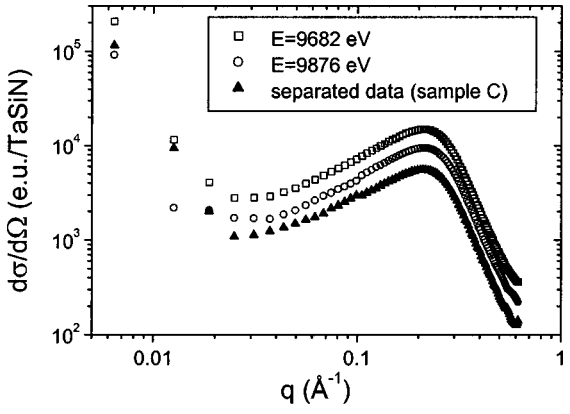

FIG. 3. Separation of the scattering curves done on sample C. Resulting intensities can be ascribed to chemical inhomogeneities, as the structural inhomogeneities contribute with an average, nonenergy-dependent scattering factor $\langle f \rangle$ and thus cancel out when performing separation.

weak maximum can be noticed at values of $2\theta \approx 60.5°$. The asymmetric broad peak can be explained in terms of chemical fluctuations in the short range order arrangement in certain regions of the matrix from which the crystalline phases are formed at higher annealing temperatures. The x-ray spectra of samples B and C, which were annealed at lower temperatures, do not significantly differ from that of sample A. Only a small decrease in the FWHM of the broadened peaks of samples B and C is observed in comparison to sample A. However, the latter three samples all show a spectrum that is typical of amorphous samples.

B. Small angle x-ray scattering (SAXS) experiments

Radial scattering intensities of the as-prepared and annealed $Ta_{40}Si_{14}N_{46}$ samples are shown in Fig. 2. The integral scattering intensities increase with higher annealing temperature proposing that the overall volume fraction of structural or chemical inhomogeneities increase with the annealing temperature. The samples annealed up to 900 °C (A–D) all show local intensity maxima in the q region 0.2 Å$^{-1} < q < 0.3$ Å^{-1}. The maximum in the radial scattering data of sample A is only weakly seen, whereas the three annealed samples B–D show a clearly visible peak. This maximum is attributed to an interparticle interference effect and the position of its maximum contains information about the interparticle distance. It should be stressed at this point that the scattering data provides information about the size of the scattering particles, even if no real particles with well-defined interfaces but only chemical fluctuations are present in the samples. The scattering contribution which is caused by the chemical variations is equal to that of virtual particles with a radius R. However, the virtual scattering radius of these chemical fluctuations can be interpreted as the characteristic length for their lateral extension.

After annealing at 950 and 1000 °C the scattering intensities dominantly increase in the lower q-value region, however, a maximum is not observed in the graph of sample F, which has a plateau-like shape around $q \approx 0.1$ Å^{-1}. In addition to that anisotropic scattering was observed on the 2D detector image at very small q values. In this q range no reliable values were obtained for the scattering curves. These data points must be excluded when numerically evaluating the scattering data, which will be discussed in more detail later.

In the performed ASAXS analyses of the samples the scattering intensities decrease monotonically when approaching the Ta-L_{III} edge. As an example, the separation procedure is shown for sample C in Fig. 3. The calculated separated scattering curves for all samples (A–F) are presented in Fig. 4 giving clear evidence for inhomogeneously distributed Ta. Obviously the shape of the separated data curves is very similar to those measured at $E=9682$ eV. This indicates that the SAXS signals, especially the intensity maximum, are produced by particle scattering and that a decomposition occurs during annealing leading to different Ta composition in the particles and the amorphous matrix.

In order to determine the size of the nanocrystals, Guinier fits were done on the scattering data from the samples E and F. For these analyses, the q range 0.018

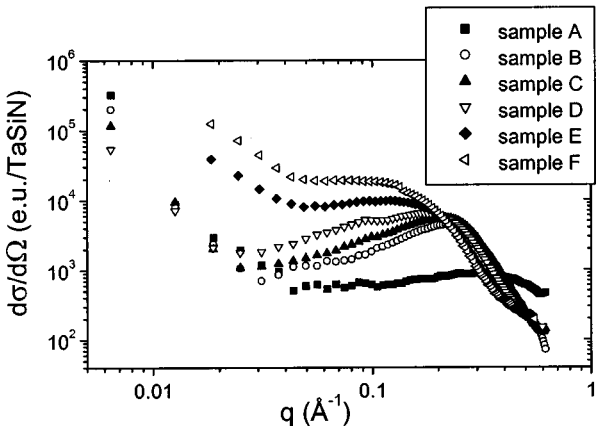

FIG. 4. Separated $Ta_{40}Si_{14}N_{46}$ scattering intensities. The curves were calculated by forming the difference of the intensities measured at $E_1=9682$ eV and $E_2=9876$ eV, for samples E and F the smaller q values are omitted because of anisotropic scattering.

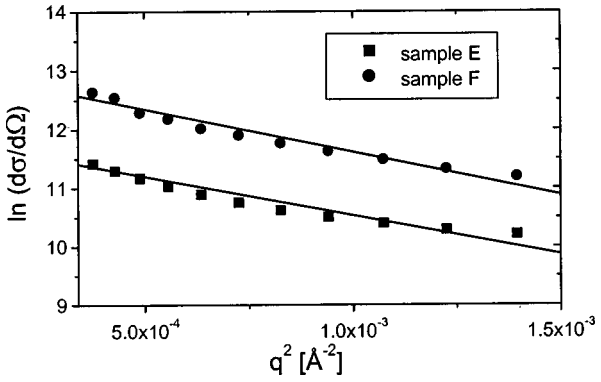

FIG. 5. Guinier fits of crystallized $Ta_{40}Si_{14}N_{46}$ samples E and F yielding the Guinier radius and thus the size of Ta_5Si_3 nanocrystals, assuming spherical symmetry for the particles. The q region used for Guinier analysis is $0.018\ \text{Å}^{-1}<q<0.04\ \text{Å}^{-1}$, so that interparticle interference contribution is assumed to be negligible.

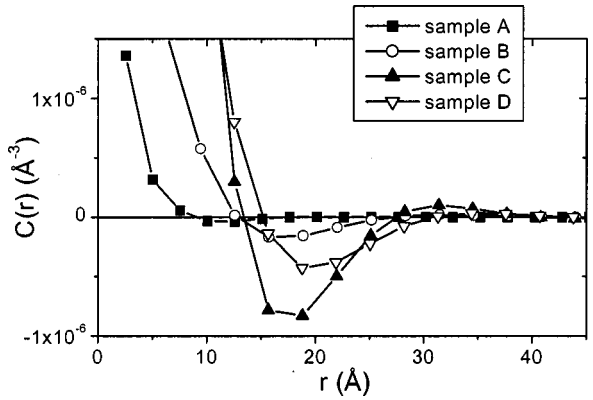

FIG. 6. Correlation functions $C(r)$ of different $Ta_{40}Si_{14}N_{46}$ samples calculated by a FFT algorithm from the original scattering curves.

$\text{Å}^{-1}<q<0.04\ \text{Å}^{-1}$ was chosen for the Guinier fits, which are shown in Fig. 5. In this q region no scattering contribution of interparticle interference is assumed. The diameters of the scattering particles were calculated from the slopes of the linear fits to be 16.3(6) nm for sample E and 17.1(6) nm and sample F, respectively. Transmission electron microscopy (TEM) analyses of these samples prove spherical symmetry of the precipitates.[19] The feasibility of Guinier analyses is an indication of the crystallinity of these two samples, which was also found by x-ray diffraction. The calculated particle sizes are matching very well with the coherence lengths of the Ta_5Si_3 peaks found by Scherrer analysis of the XRD data. However, the self-consistency requirement $qR<2$ for the feasibility of Guinier fits is not strictly fulfilled for larger q values which makes the Guinier data questionable. For the other four samples A–D it is not possible to determine a well-defined particle radius because of the nonlinear shape of the scattering data in a Guinier plot.

A more comprehensive way of scattering data evaluation if necessary, especially for the noncrystalline samples because of the above-mentioned restrictions. The correlation function $C(r)$ for electron density fluctuation is calculated from the given scattering intensity $I(q)$ by a Fourier transformation[20]

$$C(r)=\frac{1}{2\pi^2}\int_0^\infty I(q)\cdot q^2\frac{\sin(qr)}{qr}dq \equiv\langle\Delta n_f(r')\cdot\Delta n_f(r'+r)\rangle, \quad (2)$$

$\Delta n_f(r')$ is called the scattering contrast. This function can be used to calculate the distance between particles with the same sign of electron density difference relative to a homogeneous matrix, because it is the average of the product of two fluctuations at a distance r.[20]

The correlation function was calculated by a fast Fourier transform (FFT) algorithm and the results for the $Ta_{40}Si_{14}N_{46}$ samples (A–D) are shown in Fig. 6. Due to the self-correlation of the particles the $C(r)$ values are positive for small distances r. For larger values of r the curves are going through a minimum and again rising above zero, hereafter approaching zero. The zero level is determined by the average electron density of the matrix. The position of the minimum can be interpreted as the maximum size of the decomposed regions, the position of the second maximum is equal to the correlation distance of two neighboring decomposed regions with the same sign of electron density difference. From Fig. 6 it follows that the magnitude of the electron density fluctuations and also the size of the decomposed regions tend to increase with increasing annealing temperature. For sample D, however, no further increase in electron density fluctuation is observed, proposing that not only a decomposition, but also a subsequent nucleation of TaN grains could occur at a temperature of 900 °C. However, an unambiguous assignment is not possible based on the scattering and diffraction data only. The interference distance can also be estimated by the expression

$$d_{\text{corr}}=2\pi/q_{\max}, \quad (3)$$

where $q_{\max}$ is the position of the maximum in the scattering intensity curves shown in Fig. 4. The values received by Eq. (3) can be compared to the data resulting from the correlation function $C(r)$ given by Eq. (2). A comparison of the sizes of the scattering particles by Guinier analysis and the correlation function $C(r)$ to the data received by evaluating XRD data via Eq. (1) is gathered in Table II. The ratio of $p=d_{\text{corr}}/D_{\text{part}}$ is calculated from the values given in Tables II and III in order to get an idea of the packing density. This value is added in the last column of Table III, which is designated with packing parameter. The value is about $p=2$ for all investigated samples. This indicates a close packing of the particles which have formed by the decomposition process in the matrix. These results give rise to a model in which a

TABLE III. Comparison of the resulting data concerning the correlation of the particles.

$Ta_{40}Si_{14}N_{46}$ sample	$q_{\max}$ (Å^{-1})	$d_{\text{corr}}=2\pi/q_{\max}$ (nm)	d_{corr} (nm) [from $C(r)$]	Packing parameter
A	0.31	2.0	2.0	1.7
B	0.23	2.7	3.1	1.9
C	0.22	2.9	3.1	1.7
D	0.18	3.5	3.4	2.1
E	0.12	5.2	[4.5–5.5]	2.0

sphere is surrounded by a depletion shell. These shells touch each other according to the hard sphere model given by Guinier and Fournet[21] leading to a correlated spatial arrangement. In the special case of $p=d_{\mathrm{corr}}/D_{\mathrm{part}}\equiv R_{\mathrm{hs}}/R=2$, the radius of the shell is twice the radius of the particle.

C. Fitting of measured scattering curves

As another analysis method the separated scattering data of the samples A–F was fitted by the Guinier–Fournet formula, which describes interference effects in the model of hard spheres[21]

$$I(q)=N\cdot\Delta n_f^2\cdot\int_0^\infty P(r)\cdot V^2(r)\cdot S^2(q,r)\Phi(q,R_{\mathrm{hs}},\eta_{\mathrm{hs}})dr+\Pi q^{-4}, \tag{4}$$

where N is the number of scatterers, $S(q,r)$ is the structure factor of a sphere,[22] Δn_f is the scattering contrast, and $\Phi(q,R_{\mathrm{hs}},\eta_{\mathrm{hs}})$ is the interference function according to the Percus–Yevick theory.[23–25] Π is the Porod prefactor, which is added to consider the scattering intensity increase at very low q vectors, which is caused by chemical inhomogeneities larger than 50 nm. $P(r)$ is a size distribution of the particle radius, which was chosen to be a lognormal distribution[22] to avoid the presence of unphysical negative radii like Tsao *et al.*[25] used to describe the SAXS intensity for a polydisperse system of precipitations. The used lognormal distribution is given by the expression

$$P(r)=\frac{1}{\sqrt{2\pi}\cdot\sigma\cdot r_0}\cdot\exp\left(-\frac{\ln^2(r/r_0)}{2\sigma^2}\right), \tag{5}$$

where σ is the distribution width and r_0 is the center of the distribution. The fitting curve including the five fitting parameters $c_1 \ldots c_5$ can be written as

$$I(q)=c_1\cdot\int_0^\infty P(r,c_2,c_3)\cdot V^2(r)\cdot S^2(q,r)\Phi(q,2\cdot r,c_4)dr+c_5\cdot q^{-4}, \tag{6}$$

assuming twice the size of the particles for the hard spheres. For the samples E and F there was used a bimodal polydisperse model in order to take into account the appearance of the two crystalline phases (TaN and Ta_5Si_3) with different grain sizes, as found by XRD phase analysis. The results of the fitting functions together with the separated scattering data are shown in Fig. 7. A good agreement between simulated and measured data can be obtained by fitting the introduced model to the scattering data of the Ta–Si–N films proposing that the films can be described well by this model. The numerical values for the fitting variables, which are shown in Table IV, indicate that the center of the distribution gives smaller particle sizes for the Ta_5Si_3 grains of the crystalline films compared to x-ray diffraction and Guinier analysis. However, it must be noted that the lognormal distributions with the given distribution width values exhibit a long tail of larger particles contributing to the scattering intensity. The lognormal distributions of the samples A–D are plotted in Fig. 8. It has to be stressed that these distributions should not be understood as real particles, but rather as regions in the films, where the electron density differs from that of the matrix. Consequently, the plot of sample A has to be interpreted as chemical inhomogeneities on a scale smaller than $d=2r<15$ Å, where the tail of the distribution approaches zero. The size distributions from samples B and C do not significantly differ, proposing that no significant difference of the decomposition process occurs at temperatures of 800 and 850 °C. However, the size distribution of sample D shows a larger distribution width and a smaller value for the peak radius. These results are compatible with the findings of the XRD evaluation and the other results from the SAXS experiments, proving the assumption of the first onset of crystallization occurring parallel to the observed decomposition at a temperature of 900 °C.

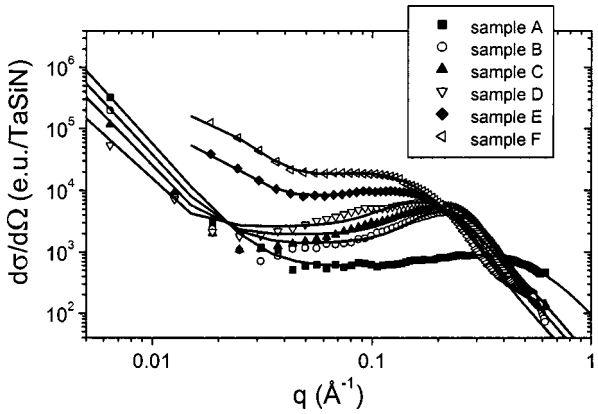

FIG. 7. Separated $Ta_{40}Si_{14}N_{46}$ scattering intensites (dots) and polydisperse fits (lines), samples E and F were fitted in the q range $q>0.018$ Å^{-1}.

We thus conclude that fitting of the radial scattering data yields results which are in good agreement with the other

TABLE IV. Results of ASAXS fits, D_1 is attributed to TaN nanocrystals and D_2 to Ta_5Si_3 nanocrystals, respectively, close packing in a fcc structure corresponds to a volume fraction of $\eta=0.74$.

Ta–Si–N sample	Center of distribution $2R_1=D_1$ (nm)	Distribution width σ_{D1}	Center of distribution $2R_2=D_2$ (nm)	Distribution width σ_{D2}	Hard sphere volume fraction η_{hs}
A	0.36	0.445			0.35
B	1.70	0.279			0.51
C	1.72	0.281			0.49
D	1.61	0.42			0.47
E	1.62	0.31	13.2	0.39	0.26
F	1.64	0.37	10.5	0.43	0.29

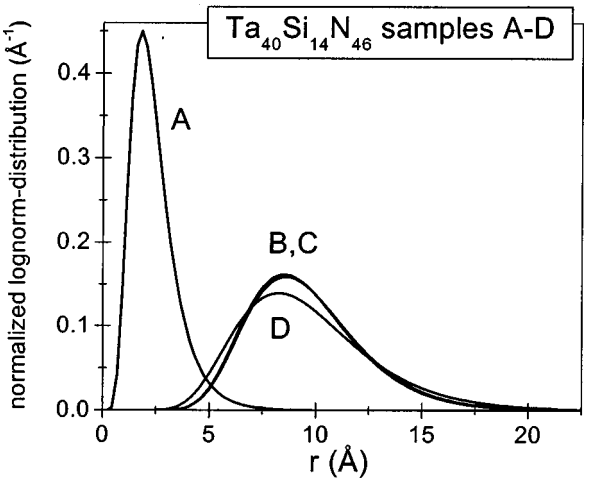

FIG. 8. Fits of lognormal size distributions of electron density fluctuations for the investigated $Ta_{40}Si_{14}N_{46}$ samples A–D.

evaluation methods and, moreover, provides additional information on the width of the size distributions of the chemical inhomogeneities and the hard sphere volume fraction.

IV. CONCLUSIONS

Anomalous small angle x-ray scattering experiments were shown to be a powerful technique for analyzing amorphous or near-amorphous films in order to acquire information about the size and correlation between decomposed regions and nanosized particles in the investigated films. It was observed that $Ta_{40}Si_{14}N_{46}$ is truly amorphous when reactively sputtered. These thin films show a decomposition when annealed at temperatures of 800 and 850 °C and first signs of nanocrystallization at 900 °C, where small grains of the TaN phase are assumed to develop in the amorphous matrix. After annealing at higher temperatures the existence of the hexagonal Ta_5Si_3 phase was found. The current investigations propose a model in which a Si outdiffusion from certain regions of the amorphous matrix occurs. This diffusion-like behavior is believed to be a self-limiting process and is stopped by an accumulative increase of Si atoms around nanoparticles, consisting of TaN-nucleation sites which crystallize after longer annealing duration. This decomposition can be considered as the detrimental factor for the failure of this diffusion barrier even before the crystallization of the sample starts. The onset of the decomposition process at temperatures of about 800–850 °C at the $Ta_{40}Si_{14}N_{46}$/Cu interface gives rise to a Si enrichment of certain regions at that interface encouraging the chemical reaction and formation of Cu_3Si nucleation sites. Once these silicide grains have formed, a rapid growth is thermodynamically favored at these temperatures leading to a deterioration of the Ta–Si–N barrier film.

ACKNOWLEDGMENTS

The authors gratefully acknowledge the financial support of the DFG via SFB345. The authors would like to thank Dr. T. Kacsich and Dr. S. Gasser for the sputter preparation of the samples.

[1] S. K. Rha, W.-J. Lee, S.-Y. Lee, D.-W. Kim, C.-O. Park, and S.-S. Chun, J. Mater. Res. **12**, 3367 (1997).
[2] S. S. Wong, C. Ryu, H. Lee, and K. W. Kwon, Mater. Res. Soc. Symp. Proc. **514**, 75 (1998).
[3] G. S. Chen, P. Y. Lee, and S. T. Chen, Thin Solid Films **353**, 264 (1999).
[4] J. O. Olowafe, C. J. Mogab, R. B. Gregory, and M. Kottke, J. Appl. Phys. **72**, 4099 (1992).
[5] J.-S. Chun, I. Petrov, and J. E. Greene, J. Appl. Phys. **86**, 3633 (1999).
[6] E. Kolawa, J. M. Molarius, C. W. Nieh, and M.-A. Nicolet, J. Vac. Sci. Technol. A **8**, 3006 (1990).
[7] T. Kacsich, S. Gasser, Y. Tsuji, A. Dommann, and M.-A. Nicolet, J. Appl. Phys. **85**, 1871 (1999).
[8] D. J. Kim, S. P. Jeong, Y. T. Kim, and J. W. Park, Mater. Res. Soc. Symp. Proc. **473**, 247 (1997).
[9] T. Hara, M. Tanaka, K. Sakiyama, S. Onishi, K. Ishihara, and J. Kudo, Jpn. J. Appl. Phys., Part 2 **36**, L893 (1997).
[10] D. E. Kotecki *et al.* IBM J. Res. Dev. **43**, 367 (1999).
[11] A. Grill, C. Jahnes, and C. Cabral, Jr., J. Mater. Res. **14**, 1604 (1999).
[12] C. Cabral, Jr., K. L. Saenger, D. E. Kotecki, and J. M. E. Harper, J. Mater. Res. **15**, 194 (2000).
[13] W. J. Dauksher *et al.*, J. Vac. Sci. Technol. B **9**, 344 (1995).
[14] D.-S. Yoon and H. K. Baik, J. Vac. Sci. Technol. B **16**, 1137 (1998).
[15] R. Ventakraman *et al.*, Mater. Res. Soc. Symp. Prov. **514**, 41 (1998).
[16] Y.-J. Lee, B.-S. Suh, M. S. Kwon, and Ch.-O. Park, J. Appl. Phys. **85**, 1927 (1999).
[17] H.-G. Haubold, K. Gruenhagen, M. Wagener, H. Jungbluth, H. Heer, A. Pfeil, H. Rongen, G. Brandenburg, R. Moeller, J. Matzerath, P. Hiller, and H. Halling, Rev. Sci. Instrum. **60**, 1943 (1989).
[18] B. D. Cullity, *Elements of X-Ray Diffraction*, 2nd ed. (Addison-Wesley, Reading, MA, 1978).
[19] M. Bicker, C. U. Pinnow, U. Geyer, and S. Schneider, Appl. Phys. Lett. **78**, 3618 (2001).
[20] O. Glatter, *Small Angle X-Ray Scattering* (Academic, London, 1982).
[21] A. Guinier and G. Fournet, *Small Angle Scattering of X-Rays* (Wiley, New York, 1955).
[22] H. G. Haubold, Einführung in die Kleinwinkelstreuung, 27. IFF Ferienkurs, Vorlesungsmanuskript C6, (1996).
[23] N. W. Ashcroft and J. Lekner, Phys. Rev. **145**, 83 (1966).
[24] J. S. Pedersen, J. Appl. Crystallogr. **27**, 595 (1994).
[25] C.-S. Tsao and T.-L. Lin, J. Appl. Crystallogr. **32**, 426 (1999).